Magnetic diversity in stable and metastable structures of CrAs

Busheng Wang,[1,2] Qing Lu,[2] Yanfeng Ge,[1] Kaicheng Zhang,[3] Wenhui Xie,[4] Wu-Ming Liu,[2,*] and Yong Liu[1,†]

[1]*State Key Laboratory of Metastable Materials Science & Technology and Key Laboratory for Microstructural Material Physics of Hebei Province, School of Science, Yanshan University, Qinhuangdao 066004, China*

[2]*Beijing National Laboratory for Condensed Matter Physics, Institute of Physics, Chinese Academy of Sciences, Beijing 100190, China*

[3]*Department of Physics, Bohai University, Jinzhou 121000, China*

[4]*Department of Physics, East China Normal University, Shanghai 200062, China*

(Received 16 May 2017; revised manuscript received 10 September 2017; published 18 October 2017)

We present results of electronic structure calculations of the bulk properties of CrAs. The crystalline structures of CrAs are investigated by the use of *ab initio* calculations with an unbiased swarm structural search under ambient and high pressure. Both the double helimagnetic and nonmagnetic phases in the neutron experiment are obtained and the pressure dependence of the magnetic phase transition is predicted. The $Pnma$ structure is the most stable structure below 33.1 GPa, meanwhile a magnetic phase transition of helimagnetic→antiferromagnetic→nonmagnetic is observed. The system tends to be antiferromagnetic after the double helimagnetic state near the optimal superconductivity regime without a crystal phase transition, which suggests that antiferromagnetic correlations between neighboring exchange interactions may be essential for the emergence of superconductivity in CrAs rather than a structural phase transition. Furthermore, the present results show that the $Pnma$ phase undergoes a pressure-induced phase transition to a cubic $P2_13$ phase at 33.1 GPa. In addition, three low-enthalpy phases with a diverse magnetic order are identified as metastable states under ambient pressure. As the analytical results of the electronic structure, the three metastable structures, $P\bar{6}m2$ type A, $P\bar{6}m2$ type B, and $P4/nmm$, are antiferromagnetic, nonmagnetic, and ferromagnetic, respectively. An explanation for the interesting difference in the spin polarization is sought, in particular, for the covalent-ionic interactions between Cr and As atoms. The present results elucidate the structural and electronic properties of CrAs, and offer major implications as regards the diverse magnetic behaviors of CrAs.

DOI: 10.1103/PhysRevB.96.134116

I. INTRODUCTION

Transition-metal pnictides have been extensively investigated for their remarkable and intriguing physical and chemical properties [1–6]. Recently, a noncollinear double helimagnetic (DHM) superconductor was obtained in a compressed chromium monoarsenide (CrAs) with a critical temperature of 2 K at $P \approx 1$ GPa [6,7], which has generated intensive research about the microscopic magnetic properties and their interplay with superconductivity [8–12]. Subsequently, a new family of quasi-one-dimensional (Q1D) superconductors $A_2Cr_3As_3$ (A = K, Rb, Cs) has been discovered at ambient pressure with T_C up to 6.1 K [13–16]. The research on the magnetic structure of CrAs has a long history [17–19]. CrAs undergoes a first-order transition at $T_N \approx 265$ K into an antiferromagnetic (AFM) state, where the magnetic propagation vector k is found to be parallel to the c axis and the magnetic moments lie in the ab plane. This first-order magnetic phase transition is accompanied by abrupt changes in the lattice parameters, especially the sudden expansion of b below T_N [19]. Very recently, in the experimental studies of Wu *et al.* [6] and Kotegawa *et al.* [7], the resistivity of CrAs is suppressed progressively under pressure and disappears at a critical pressure $P_c \approx 0.7$ GPa. Obviously, the magnetic phase-transition temperature T_N drastically decreases with pressure, whereas the magnetism completely disappears above the critical pressure P_c. Moreover, neutron diffraction measurements have provided a precise determination of the magnetic structure and revealed marginal changes in the magnetic structure with pressures up to 0.65 GPa, but the magnetic ordering moments are partially suppressed [10].

Previous research on unconventional superconductors implied that external pressure remarkably adjusts their magnetic and crystal structures, consequently effecting their physical behaviors, such as the appearance of superconductivity [11,20]. Shen *et al.*'s [11] neutron experiments show that nearest-neighbor spins tend to be aligned antiparallel near the optimal superconductivity regime, which suggests that AFM correlations between nearest neighbors may be essential for superconductivity. Very recently, Yu *et al.* [20] predicted that manganese monophosphide (MnP) undergoes a remarkable pressure-induced structural phase transition under pressure, with an extensive crystal structure search and first-principles calculations. However, little attention has been devoted to consider the various types of magnetism during structural optimization. We aim to study the pressure dependence of the magnetic and crystal structures of CrAs within structural search and first-principles calculations. It is hoped that the understanding of microscopic magnetics and their interplay with superconductivity will be more clear with our proposed approach.

In this paper, we study the magnetic and crystal structures of CrAs utilizing first-principles calculations. We derive the pressure evolution of the magnetic order and crystal structures of CrAs, obtain both the DHM and nonmagnetic (NM) phase of $Pnma$ in the neutron experiments [6,7,11], and predict correctly the pressure dependence of the magnetic phase transition (DHM → AFM →NM), in good agreement with

*wliu@iphy.ac.cn
†ycliu@ysu.edu.cn

the overall trend observed in neutron experiments [11]. The results imply that AFM correlations between neighboring exchange interactions may be essential for superconductivity. We further show that the $Pnma$ structure is the most stable structure below 33.1 GPa. Then, pressure induces phase transitions from $Pnma$ to a cubic $P2_13$ structure at 33.1 GPa. Furthermore, three low-enthalpy phases, $P\bar{6}m2$ type A, $P4/nmm$, and $P\bar{6}m2$ type B, for CrAs with diverse magnetic orders are identified as metastable states under ambient pressure. The electronic structural calculations show the metallicity of the concerned phases, and the absence of any imaginary frequencies of phonon spectra ensures lattice structure stability. A further analysis of the bonding nature shows that charges conglomerate between the Cr and As atoms and form weak covalent Cr-As bonds. An explanation of the interesting difference in the spin polarization is sought, in particular, for covalent-ionic interactions between Cr and As atoms. The variable magnetic properties make CrAs an exciting platform to deeply understand the correlation of magnetic, structural, and superconductive properties.

II. COMPUTATIONAL DETAILS

Our structural prediction of CrAs under ambient pressure is investigated by globally minimizing the potential energy surface via a swarm-intelligence-based CALYPSO method [21,22] in combination with *ab initio* density functional theory (DFT) total-energy calculations. Its validity in rapidly finding stable ground-state structures has been demonstrated by applications in various material systems ranging from elements to binary and ternary compounds [21,23–25]. The underlying energetic calculations are performed with the plane-wave pseudopotential method as implemented in the VASP code [26,27]. The Perdew-Burke-Ernzerhof (PBE) [28] generalized gradient approximation is chosen for the exchange-correlation function. The electron-ion interaction was described by the projected augmented-wave (PAW) [29] potentials with $3d^5 4s^1$ and $4s^2 4p^3$ as valence electrons for Cr and As, respectively. The structural search of CrAs is performed with simulation cells containing one to eight formula units. During the structural search, an economical set of parameters is used to evaluate the relative enthalpies of the sampled structures on the potential energy surface, following which a kinetic cutoff energy of 700 eV for the expansion of the wave function and Monkhorst-Pack k meshes with a grid spacing of $2\pi \times 0.03$ Å^{-1} are then adopted to ensure the enthalpy converges to better than 1×10^{-5} eV per cell. Four magnetic phases (collinear NM, FM, AFM, and noncollinear DHM with spins propagating on the ab plane) are considered during structural relaxations. The calculations of the phonon spectra are performed using the density functional perturbation theory [30–32] with VASP and PHONOPY codes [33,34].

III. RESULTS AND DISCUSSION

A. Structural prediction and stability analysis under ambient pressure

In atmospheric pressure, CrAs stabilizes in the MnP phase (space group $Pnma$, No. 62), and other stoichiometries are possibly present in small traces in single-crystal samples of

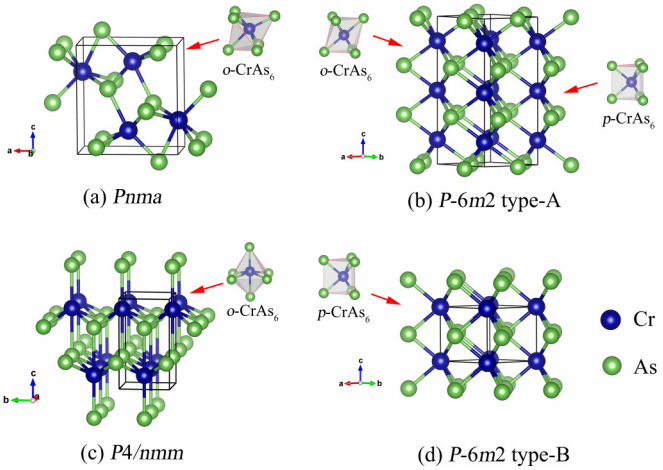

FIG. 1. Three-dimensional schematic representations of the stable and metastable phases for CrAs. (a) $Pnma$, (b) $P\bar{6}m2$ type A, (c) $P4/nmm$, and (d) $P\bar{6}m2$ type B. Blue atoms depict Cr, while green atoms represent As. Schematics of the structural polytypes: o-$CrAs_6$ (the Cr atom is coordinated to six As atoms in an octahedral coordination), and p-$CrAs_6$ (the Cr atom is coordinated to six As atoms in a triangular prismatic coordination).

CrAs [35]. In the MnP phase, the Cr atoms are octahedrally coordinated with six As atoms, and lie in a zigzag line along the a axis and c axis [Fig. 1(a)].

In the present section, we focus on CrAs with different magnetic states under ambient pressure. The thermodynamic stabilities of CrAs are evaluated by their formation enthalpies (ΔH) relative to the products of dissociation into constituent elements (solidified phases of Cr and As),

$$\Delta H = [h(\mathrm{CrAs}) - h(\mathrm{Cr}) - h(\mathrm{As})]/2, \quad (1)$$

where h is the absolute enthalpy corresponding to the most stable magnetic state. The results of the predicted structure are summarized in the convex hulls constructed with a solid $Im\bar{3}m$ phase of Cr [36] and $R\bar{3}m$ phase of As [37] as the binary compound, as depicted in Fig. S1 in the Supplemental Material [38].

The negative value of formation enthalpy indicates that solid Cr and As will react to form a compound, and for the positive value, the compound is expected to decompose into Cr and As. Knowing only the chemical compositions, we correctly reproduced the experimental $Pnma$ phase [18,39] at ambient pressure. As the $Pnma$ phase emerges on the convex hull, it validates the effectiveness of the CALYPSO methodology in structural searches of CrAs. More importantly, $P6_3/mmc$, $P\bar{6}m2$ type A, and $I4_1/md$ with an AFM state, $P4/nmm$ with a ferromagnetic (FM) state, and $P\bar{6}m2$ type B with a NM state are energetically favored over elemental dissociation. Besides, the $F\bar{4}3m$, $P63mc$, and $Pm\bar{3}m$ phases are unstable against elemental dissociation. But the thin film of the $F\bar{4}3m$ phase still has been fabricated with the help of GaAs(001) substrates by molecular beam epitaxy (MBE) [40–43]. Finally, the analysis of the predicted structures provides a short list of candidate structures with space group $Pnma$, $P\bar{6}m2$ type A, $P4/nmm$, and $P\bar{6}m2$ type B. (Due to dynamic instability, the

TABLE I. Lattice parameters and atomic positions of CrAs with the ground magnetic state. The structures were optimized at a higher level of accuracy. Only the fractional coordinates of symmetry inequivalent atoms are reported. The numbers of atoms in a conventional cell are given.

Space group atom	Magnetic state	Lattice parameters (Å, deg)	Atomic positions (fractional)	ΔH (eV)
$Pnma$ 8	DHM	$a = 5.617$ $b = 3.552$ $c = 6.187$ $\alpha = \beta = \gamma = 90$	Cr 4c (0.5070 0.7500 0.2093) As 4c (0.2091 0.2500 0.5856)	−0.228
$P\bar{6}m2$ type A 6	AFM	$a = b = 3.512$ $c = 8.940$ $\alpha = \beta = 60$ $\gamma = 120$	Cr 2a (0.0000 0.0000 0.1665) Cr 1b (0.0000 0.0000 0.5000) As 2h (0.3333 0.6667 0.3337) As 1e (0.6667 0.3333 0.0000)	−0.125
$P4/nmm$ 4	FM	$a = b = 3.573$ $c = 5.087$ $\alpha = \beta = \gamma = 90$	Cr 2c (0.0000 0.5000 0.6942) As 2c (0.0000 0.5000 0.2039)	−0.075
$P\bar{6}m2$ type B 4	NM	$a = b = 3.226$ $c = 3.165$ $\alpha = \beta = 60$ $\gamma = 120$	Cr 1a (0.0000 0.0000 0.0000) As 1d (0.3333 0.6667 0.5000)	−0.073

results of $P6_3/mmc$ and $I4_1md$ are shown in the Supplemental Material [38].)

The structures of selected phases are shown in Fig. 1. The lattice parameters and atomic positions of different structures are summarized in Table I. The most energetically stable CrAs was predicted to crystallize in an MnP-type structure with space group $Pnma$ [Fig. 1(a)], consisting of As-sharing $CrAs_6$ irregular octahedrons, and the central Cr atom octahedrally coordinated with six As atoms, named o-$CrAs_6$. As the neutron experiments [18,19] report, a $Pnma$ phase with DHM order propagating along the c axis is obtained in our calculations, shown in Fig. 2. Detailed information is presented in the Supplemental Material [38].

For the case of $P\bar{6}m2$ type A (3 f.u./cell) [Fig. 1(b)], the formation enthalpy is 103 meV higher than that of the $Pnma$ phase. There are two different types of polyhedrons, o-$CrAs_6$ with octahedral coordination and p-$CrAs_6$ with trigonal prismatic coordination, whose sequence is along the c axis, as shown in Fig. 1(b). The optimized structural parameters of the $P\bar{6}m2$ type-A structure are $a = b = 3.521$ Å and $c = 8.963$ Å. The primitive cell has two inequivalent Cr atoms and As atoms (labeled Cr_1 and Cr_2, As_1 and As_2). Cr_1 and Cr_2 atoms locate at crystallographic sites 2g (0.0000 0.0000 0.1665) and 1b(0.0000 0.0000 0.5000) (Wyckoff notation), whereas As_1 and As_2 atoms occupy 2h(0.3333 0.6667 0.3337) and 1e (0.6667 0.3333 0.0000), respectively. The Cr_1, As_1, and As_2 constitute the o-$CrAs_6$ polyhedron of $P\bar{6}m2$ type A, and Cr_2 and As_1 form the p-$CrAs_6$ polyhedron.

Next, the enthalpy of the $P4/nmm$ structure [Fig. 1(c)] is predicted to be 50 meV higher than that of the $P\bar{6}m2$ type-A structure. The optimized lattice parameters for the $P4/nmm$ phase are $a = b = 3.575$ Å and $c = 5.085$ Å, with one Cr atom [2c (0.0000 0.5000 0.6954)] and one As atom [2c (0.0000 0.5000 0.2049)]. Similar to the $Pnma$ phase, $P4/nmm$ consists of As-sharing o-$CrAs_6$ irregular octahedrons. The calculated Cr-As bond length is 2.578 Å, which is the longest among the selected phases for CrAs.

Further, a simple hexagonal $P\bar{6}m2$ type-B structure (1 f.u./cell) [Fig. 1(d)] is predicted to consist of p-$CrAs_6$ polyhedrons with AA stacking [Fig. 1(d)]. There is only one

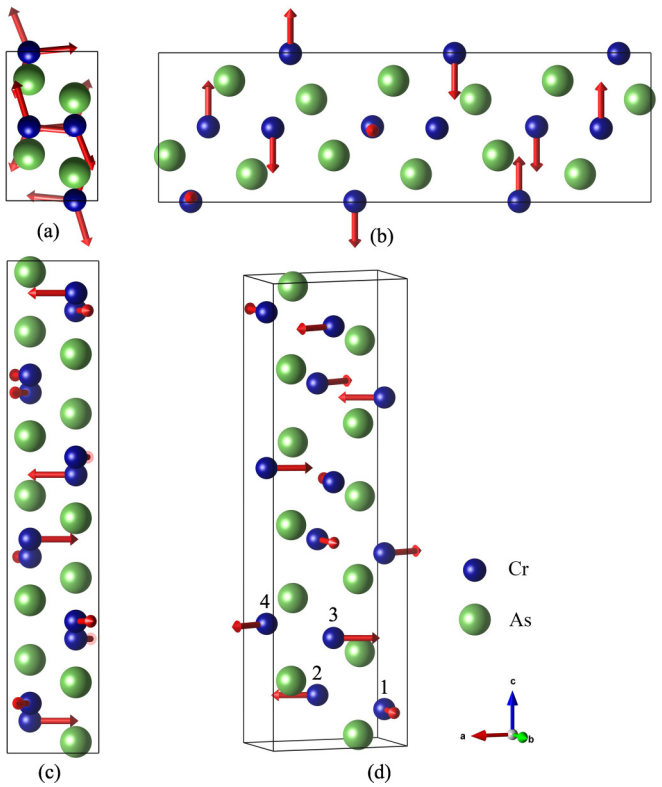

FIG. 2. Helimagnetic structure of MP-type CrAs. The magnetic moments of Cr atoms are represented by red arrows, and the evolution of the moments is shown for three unit cells along c. (a)–(c) are helical magnetic structures viewed from the c, b, and a axis, respectively, and (d) is a solid view. Blue atoms depict Cr, while green atoms represent As.

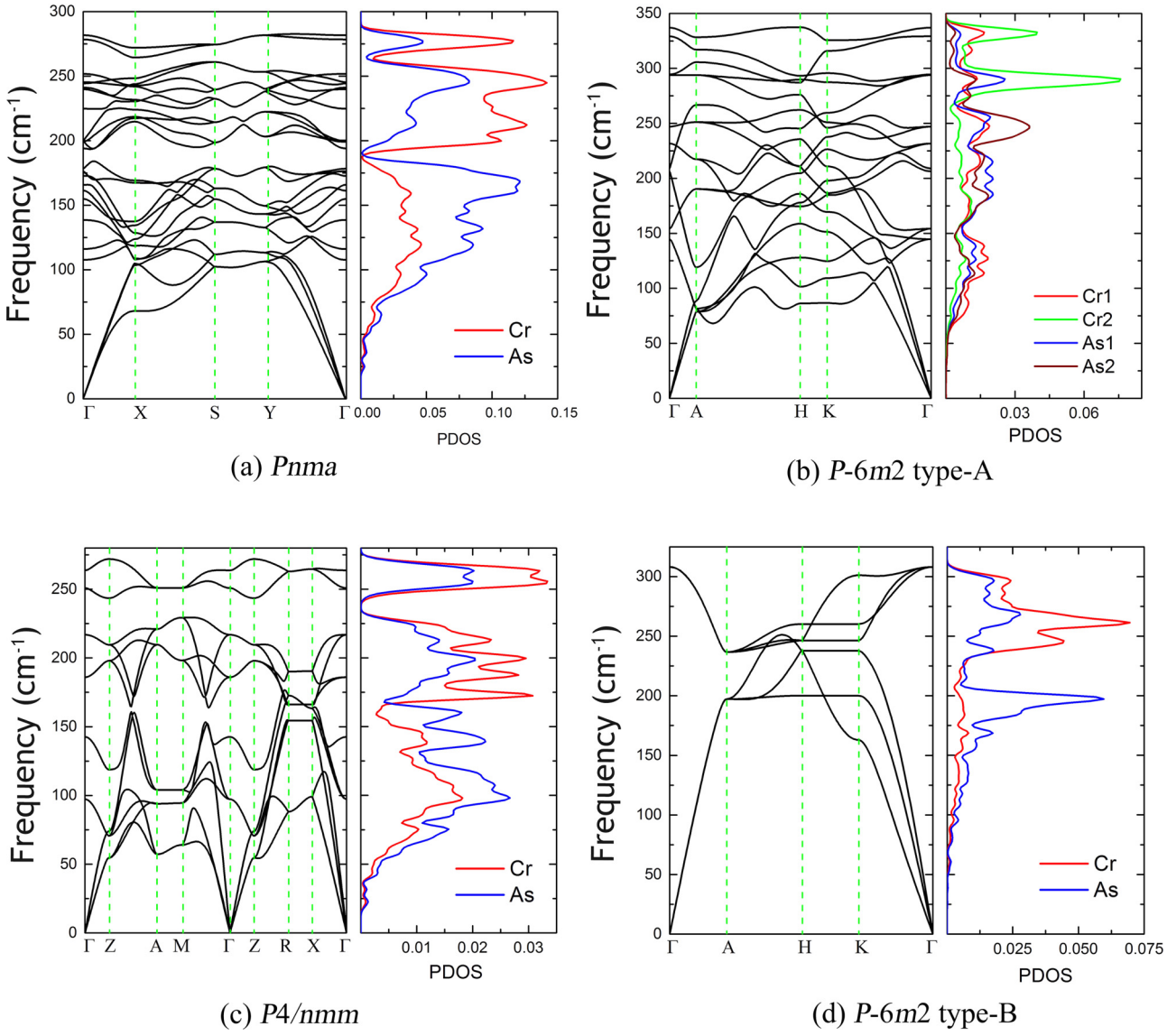

FIG. 3. Phonon spectra and phonon projected density of states (PDOS) of CrAs. (a) $Pnma$, (b) $P\bar{6}m2$ type A, (c) $P4/nmm$, and (d) $P\bar{6}m2$ type B. The absence of imaginary phonon frequencies in the entire Brillouin zone confirms the dynamical stability. The unit of phonon PDOS is states/cm^{-1} per atom.

CrAs unit in the primitive cell with $a = b = 3.226$ Å and $c = 3.165$ Å. Cr and As atoms occupy $1a$ (0 0 0) and $1d$ (0.3333 0.6667 0.5000), respectively. The shorter Cr-As bond length (2.444 Å) than that in the $P\bar{6}m2$ type-A structures (2.521 Å) demonstrates a relatively strong Cr-As interaction in the $P\bar{6}m2$ type-B structure.

For the dynamical stability of the studied structures, Fig. 3 presents the calculated phonon spectra and projected phonon density of states (PDOS) of the $Pnma$, $P\bar{6}m2$ type-A, $P4/nmm$, and $P\bar{6}m2$ type-B phases. The absence of any imaginary phonon frequencies in the entire Brillouin zone confirms the dynamical stability of the four phases. However, the appearance of imaginary phonon frequencies indicates that the $P6_3/mmc$ [44,45] Fig. S5(b) [38] and $I4_1md$ [Fig. S5(d) [38]] phases are dynamically unstable. In the phonon spectra, the relative low-frequency modes mainly originate from the heavier As atoms, and the high-frequency modes are from the lighter Cr atoms.

B. Electronic and magnetic properties

The results of electronic band structures suggest that three cases ($P\bar{6}m2$ type A, $P4/nmm$, and $P\bar{6}m2$ type B) are metallic (Fig. 4) and the electronic DOS around the Fermi level mainly comes from the Cr atoms. For the $P\bar{6}m2$ type-A phase, a flat part of the conduction band along the $\Gamma \rightarrow A$ direction results in a peak of electronic DOS at the Fermi level, as shown in Fig. 4(a). Near the Fermi level, the electronic DOS is dominated by the Cr $3d$ states with a slight contribution from the As $4p$ states, whereas the Cr1 atoms in o-CrAs$_6$ contribute more to the DOS than Cr2 atoms in p-CrAs$_6$. For the $P4/nmm$ phase, spin-up states of Cr $3d$ dominate the DOS in the energy region below the Fermi level, whereas spin-down states dominate the DOS above the Fermi level [Fig. 4(b)]. It is noteworthy that the calculation of spin polarization suggests the FM state for the $P4/nmm$ phase. For the NM $P\bar{6}m2$ type-B phase [Fig. 4(c)], a pseudogap is observed below the Fermi level (~ -1.6 eV). Near the Fermi level, the electronic DOS is

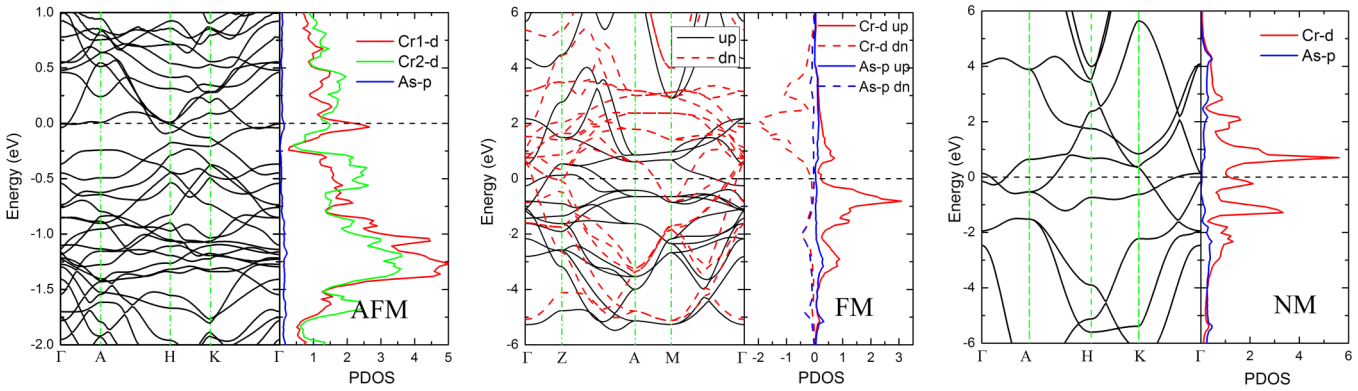

(a) *P*-6*m*2 type-A (b) *P*4/*nmm* (c) *P*-6*m*2 type-B

FIG. 4. The electronic structures of CrAs. (a) $P\bar{6}m2$ type-A phase, where the partial density of states for two inequivalent Cr atoms and As atom are represented by red, green, and red solid lines. (b) $P4/nmm$ phase, where the electronic band structure for majority spin and minority spin is represented by black solid lines and red dotted lines, while the partial density of states for the majority-spin states of the Cr and As atoms are presented by red and blue solid lines, and the majority-spin states of the Cr and As atoms are presented by red and blue dotted lines. (c) $P\bar{6}m2$ type-B phase. The Fermi level is set to zero, and the unit of electronic projected density of states (PDOS) is states/eV/atom.

dominated by the Cr 3*d* states with a slight contribution from the As 4*p* states.

In order to gain further insight into the bonding nature and analyze the ionic or covalent character, we also calculated the electron localization function (ELF) [46–48], defined as

$$\mathrm{ELF} = \frac{1}{1+(D/D_h)^2}, \tag{2}$$

$$D = \frac{1}{2}\sum_i |\nabla\phi_i|^2 - \frac{1}{8}\frac{|\nabla\rho|^2}{\rho}, \tag{3}$$

$$D_h = \frac{3}{10}(3\pi^2)^{2/3}\rho^{5/3}, \tag{4}$$

where ϕ_i is the Kohn-Sham orbital, and ρ is the local density. The ELF values of 0 and 1 correspond to perfect delocalization and localization, respectively. Figure 5 shows the results of ELF for the (110) planes of $P\bar{6}m2$ type A, $P4/nmm$, and $P\bar{6}m2$ type B. The maximum ELF value between Cr and As is about 0.8, indicating a weak covalentlike nature of the Cr-As bond. Obviously, the $P\bar{6}m2$ type-B phase possesses a relatively larger ELF value between the Cr-As covalent bond, indicating stronger localized characters [Fig. 5(c)]. Evidently, both the covalent bonding interaction and ionic bonding interaction depend sensitively on the distance between two neighboring atoms ($d_{\text{Cr-As}}$). The shorter $d_{\text{Cr-As}}$ (2.444 Å) of $P\bar{6}m2$ type B results in an enhancement of the covalent bonding interaction and reduction of the ionic bonding interaction. This demonstrates a relatively strong Cr-As covalent bond in the $P\bar{6}m2$ type-B structure.

In order to understand the bonding nature more clearly, we have calculated the charge density difference of $P\bar{6}m2$ type-A, $P4/nmm$, and $P\bar{6}m2$ type-B phases [Figs. 6(a)–6(c)]. It is noticed that electrons transfer from the Cr atom and distribute between Cr and As atoms, indicating their covalent interaction. Overall, the ELF and the charge density difference analysis results reveal that weak covalent bonds were formed between Cr and As.

Furthermore, due to the *d* orbit of the Cr atom, magnetism is expected for the CrAs compounds. The magnetic moment can be determined by the competition between two distinct

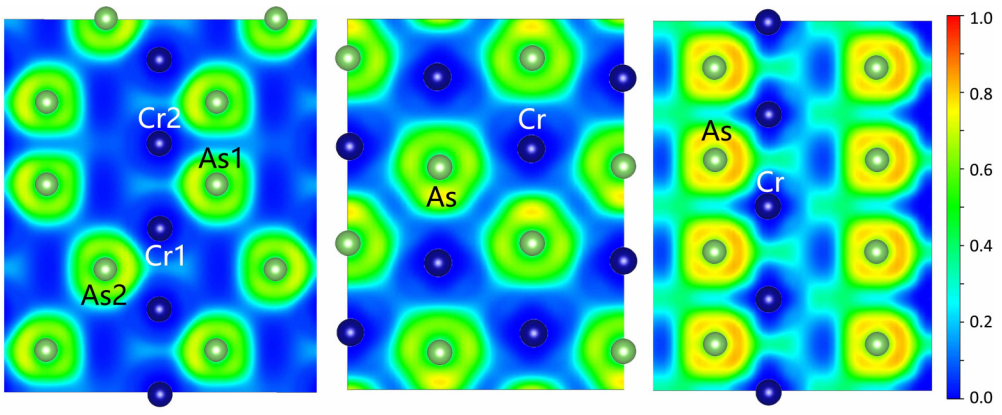

(a) *P*-6*m*2 type-A (b) *P*4/*nmm* (c) *P*-6*m*2 type-B

FIG. 5. Electron localization function (ELF) maps of CrAs. (110) plane of (a) $P\bar{6}m2$ type A, (b) $P4/nmm$, and (c) $P\bar{6}m2$ type B. The maximum ELF value between Cr and As is about 0.8, indicating a weak covalentlike nature of the Cr-As bond. Blue and green balls indicate Cr and As atoms, respectively.

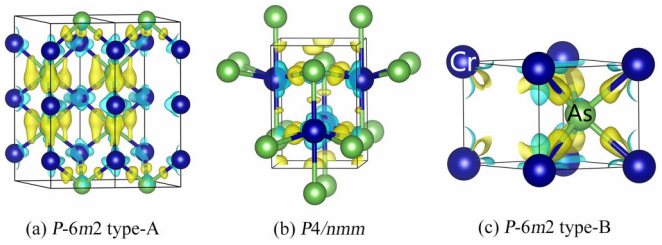

FIG. 6. Three-dimensional charge density difference with the isosurface of CrAs. (a) $P\bar{6}m2$ type A, (b) $P4/nmm$, and (c) $P\bar{6}m2$ type B. Turquoise and yellow regions indicate depletion and accumulation of electrons, respectively. The isosurface plots (with a value of 0.01 e/bohr^3) clearly illustrate the charge transfer from the Cr atom and distribution localized between Cr and As atoms, indicating a covalent interaction for all the phases. Blue and green balls indicate Cr and As atoms, respectively.

interactions of the Cr and As atoms: covalent and ionic bonding interactions. The $d_{\text{Cr-As}}$ of the $P4/nmm$ (2.566 Å) and $P\bar{6}m2$ type-A (2.526 Å) phase are relatively longer than that of the $P\bar{6}m2$ type-B phase. The elongation of $d_{\text{Cr-As}}$ results in a reduction of the covalent bonding interaction, contrary to the ionic bonding interaction. Accordingly, the unpaired electrons accumulated on the Cr and As atoms increase slightly, leading to a variation of magnetism. However, the Cr atoms in the

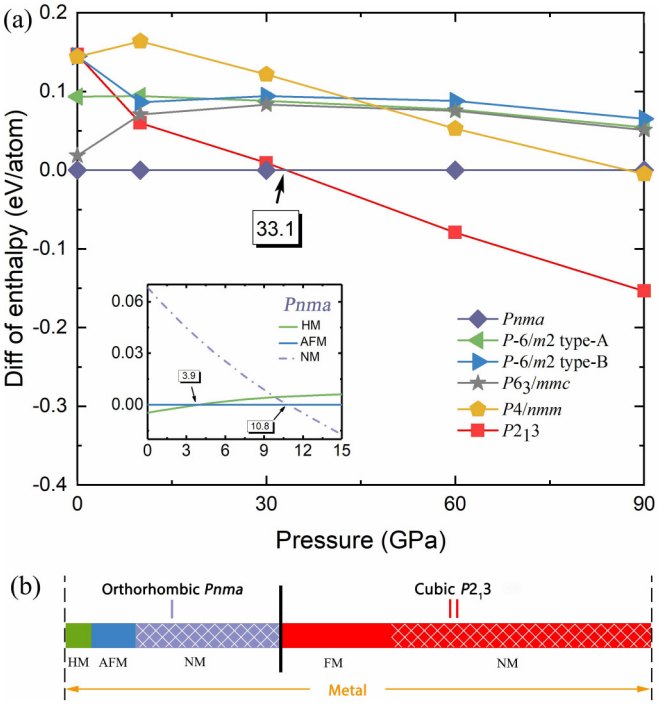

FIG. 7. (a) Relative enthalpy per atom as a function of pressure for CrAs, referenced to the $Pnma$ structure. The phase-transition series orthorhombic $Pnma$ phase to cubic $P2_13$ phase (33.1 GPa). Further calculations determined the stability of the $P2_13$ phase up to 90 GPa. The inset shows the enthalpy of various types of magnetism for $Pnma$ as a function of pressure. The $Pnma$ phase changes magnetic ordering from double helimagnetic ordering to antiferromagnetic ordering (3.9 GPa) to nonmagnetic ordering (10.8 GPa). (b) Magnetic and structural phase-transitional diagram under pressure.

TABLE II. Magnetic and lattice parameters of CrAs under ambient and applied pressure.

Space group	Magnetic state	a (Å)	b (Å)	c (Å)	P (GPa)
$Pnma$	DHM	5.617	3.552	6.187	0
$Pnma$	DHM	5.577	3.525	6.139	2
$Pnma$	AFM	5.430	3.530	5.985	5
$Pnma$	NM	5.583	3.130	5.996	15
$P2_13$	FM	4.518	4.518	4.518	40
$P2_13$	NM	4.436	4.436	4.436	60

p-CrAs$_6$ polyhedral of $P\bar{6}m2$ type B form a strong ligand field, due to the Cr-As covalent bond, thus quenching the magnetism, which also occurs in other transition-metal atoms [49,50].

C. Magnetic and structural phase diagram under pressure

In order to clarify the relation between the magnetism, structure, and superconductivity in CrAs under pressure, we extend the structural search from ambient to applied pressure. Due to the magnetic diversity in variable structures as discussed above, we consider various magnetic orderings during structural relaxation under pressure. Several candidates for the high-pressure phases are produced, and the enthalpies per atom versus pressure curves of selected structures are plotted in Fig. 7(a). The refined structural and magnetic parameters at representative pressures are given in Table II.

The $Pnma$ structure (referred to as phase I) is the most stable structure below 33.1 GPa. It is interesting to note that the $Pnma$ phase changes magnetic ordering under pressure, the DHM order is the most stable state below 3.9 GPa, followed by the AFM order (3.9–10.8 GPa), and then the NM order predominates in the pressure range from 10.8 to 33.1 GPa, as shown in the inset graphs of Fig. 7(a). The magnetic phase transition of DHM → AFM →NM in the $Pnma$ structure is in good agreement with experimental results [11], which report that the moments between nearest neighbors tend to be antiferromagnetically aligned in the bulk superconductivity regime. It should be noted that the critical pressure in our computational results (3.9 GPa) is inconsistent with the experimental results (0.7 GPa). As we concentrate on only four magnetic phase (collinear NM, FM, AFM, and noncollinear DHM with spins propagating on the ab plane), we note the limitations of the DFT method in dealing with complicated magnetic systems under temperature. Notwithstanding, our study does obtain both the DHM and NM phase in the neutron experiment [6,7,51] and predicts correctly the pressure dependence of the magnetic phase transition (DHM → AFM → NM). Furthermore, we also notice that the pressure dependence of the lattice parameters in a magnetically order state displays a clear anomaly at the critical pressure $P_c = 3.9$ GPa, as shown in Fig. 8(c), which corresponds to the magnetic phase transition. This result implies a strong coupling between magnetic and lattice degrees of freedom. The system tends to be AFM after DHM state near the optimal superconductivity regime without a crystal phase transition, and thus we suggest that AFM correlations between neighboring exchange interactions may be essential

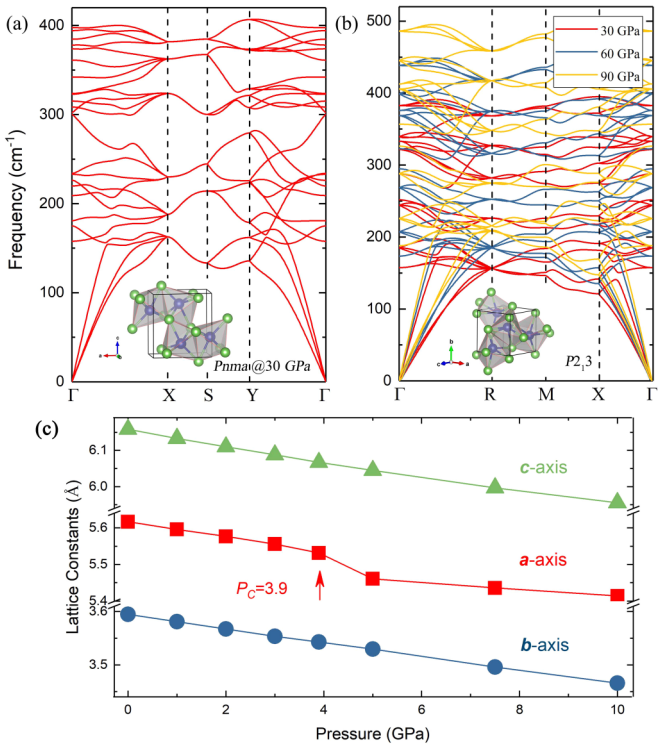

FIG. 8. Phonon spectra for the high-pressure phases of (a) $Pnma$ at 30 GPa and (b) $P2_13$ phase at 30, 60, and 90 GPa. The inset shows schematic representations of the $Pnma$ and $P2_13$ phase, respectively. (c) Pressure dependence of the lattice parameter in the magnetically ordered state.

for the emergence of superconductivity in CrAs rather than a structural phase transition.

With further compression, pressure induces phase transitions from a $Pnma$ to cubic $P2_13$ structure (referred as phase II), which predominates in the pressure range of 33.1–90 GPa. It is noted that as the neighbor number of Cr increased from six ($Pnma$ phase) to seven, the same character with MnP under pressure [20]. For the $P2_13$ phase, FM is the most stable state above 33.1 GPa, and then is quenched to zero with an increase in pressure. The NM order of the $P2_13$ phase predominates in the pressure range of around 50–90 GPa. The dynamical stability of the $Pnma$ and $P2_13$ phases under high pressure is investigated by calculating the phonon dispersion, as shown in Figs. 8(a) and 8(b). The absence of any imaginary phonon frequencies in the entire Brillouin zone confirms the dynamical stability of these two phases at 30 and during 30–90 GPa, respectively. The electronic band structures show a good metallic feature for CrAs (see Supplemental Fig. S7 [38]) in the whole pressure range we studied.

IV. CONCLUSION

In summary, we have extensively investigated the magnetic, crystal structures, phonon spectra, and electronic properties of CrAs using first-principles calculations. We obtain both the DHM and NM phase in a neutron experiment and predict the pressure dependence of the magnetic phase transition (DHM→AFM→NM). The system tends to be AFM after the DHM state near the optimal superconductivity regime without a crystal phase transition, so we suggest that AFM correlations between neighboring exchange interactions may be essential for the emergence of superconductivity in CrAs rather than a structural phase transition. Furthermore, we derive the pressure evolution of the crystal structures of CrAs. The $Pnma$ structure is the most stable structure below 33.1 GPa. Then, pressure induces phase transitions from the $Pnma$ to cubic $P2_13$ structure. The ferromagnetic (FM) state is the most stable state of the cubic $P2_13$ structure above 33.1 GPa, which is then quenched to zero at around 50 GPa. In addition, three metastable phases, $P\bar{6}m2$ type A, $P4/nmm$, and $P\bar{6}m2$ type B, are predicted with diverse magnetism at ambient pressure. $P\bar{6}m2$ type A is AFM, and $P4/nmm$ and $P\bar{6}m2$ type B are FM and NM, respectively. An explanation of the interesting difference in the spin polarization is sought, in particular, for covalent-ionic interactions between Cr and As atoms. Unpaired electrons accumulate on the Cr and As atoms, leading to interesting variations in magnetism. The variable magnetic properties make CrAs an exciting platform to deeply understand the correlation of the magnetic, structural, and superconductive properties.

ACKNOWLEDGMENTS

This work was supported by the NKRDP under Grant No. 2016YFA0301500, NSFC under Grants No. 11504027, No. 11434015, No. 61227902, No. 61378017, and No. KZ201610005011, SKLQOQOD under Grant No. KF201403, and SPRPCAS under Grants No. XDB01020300 and No. XDB21030300. W.X. acknowledges the sponsorship of the Natural Science Foundation of Shanghai (Grant 15ZR1411400). Y.L. acknowledges support by the Natural Science Foundation of Hebei Province (No. A2011203037) and Key Project of Heibei Educational Department, China (No. ZD2014015).

[1] *Electronic Structure and Magnetism of 3d-Transition Metal Pnictides*, edited by K. Motizuki, H. Ido, T. Itoh, and M. Morifuji, Springer Series in Materials Science Vol. 131 (Springer, Berlin, 2009), pp. 1–142.

[2] Z. K. Liu, L. X. Yang, Y. Sun, T. Zhang, H. Peng, H. F. Yang, C. Chen, Y. Zhang, Y. F. Guo, D. Prabhakaran, and M. Schmidt, Nat. Mater. **15**, 27 (2015).

[3] G. Y. Gao, K. L. Yao, E. Sasioglu, L. M. Sandratskii, Z. L. Liu, and J. L. Jiang, Phys. Rev. B **75**, 174442 (2007).

[4] Y. Kamihara, T. Watanabe, M. Hirano, and H. Hosono, J. Am. Chem. Soc. **130**, 3296 (2008).

[5] J. F. Ge, Z. L. Liu, C. Liu, C. L. Gao, D. Qian, Q. K. Xue, Y. Liu, and J. F. Jia, Nat. Mater. **14**, 285 (2015).

[6] W. Wu, J. Cheng, K. Matsubayashi, P. Kong, F. Lin, C. Jin, N. Wang, Y. Uwatoko, and J. Luo, Nat. Commun. **5**, 5508 (2014).

[7] H. Kotegawa, S. Nakahara, H. Tou, and H. Sugawara, J. Phys. Soc. Jpn. **83**, 093702 (2014).

[8] M. R. Norman, Physics **8**, 24 (2015); J. G. Cheng, K. Matsubayashi, W. Wu, J. P. Sun, F. K. Lin, J. L. Luo, and Y. Uwatoko, Phys. Rev. Lett. **114**, 117001 (2015).

[9] H. Kotegawa, S. Nakahara, R. Akamatsu, H. Tou, H. Sugawara, and H. Harima, Phys. Rev. Lett. **114**, 117002 (2015).

[10] L. Keller, J. S. White, M. Frontzek, P. Babkevich, M. A. Susner, Z. C. Sims, A. S. Sefat, H. M. Rønnow, and C. Rüegg, Phys. Rev. B **91**, 020409(R) (2015).

[11] Y. Shen, Q. Wang, Y. Hao, B. Pan, Y. Feng, Q. Huang, L. W. Harriger, J. B. Leao, Y. Zhao, R. M. Chisnell, J. W. Lynn, H. Cao, J. Hu, and J. Zhao, Phys. Rev. B **93**, 060503(R) (2016).

[12] R. Khasanov, Z. Guguchia, I. Eremin, H. Luetkens, A. Amato, P. K. Biswas, C. Rüegg, M. A. Susner, A. S. Sefat, N. D. Zhigadlo, and E. Morenzoni, Sci. Rep. **5**, 13788 (2015).

[13] X. X. Wu, F. Yang, C. C. Le, H. Fan, and J. P. Hu, Phys. Rev. B **92**, 104511 (2015).

[14] L. D. Zhang, X. X. Wu, H. Fan, F. Yang, and J. P. Hu, Europhys. Lett. **113**, 37003 (2016).

[15] J.-J. Miao, F.-C. Zhang, and Y. Zhou, Phys. Rev. B **94**, 205129 (2016).

[16] Y. Zhou, C. Cao, and F. C. Zhang, Sci. Bull. **62**, 208 (2017).

[17] H. Watanabe, N. Kazama, Y. Yamaguchi, and M. Ohashi, J. Appl. Phys. **40**, 1128 (1969).

[18] K. Seite, A. Kjekshus, W. E. Jamison, A. F. Andresen, and J. E. Engebretsen, Acta Chem. Scand. **25**, 1703 (1971).

[19] H. Boller and A. Kallel, Solid State Commun. **9**, 1699 (1971).

[20] Z. Yu, W. Wu, P. X. Lu *et al.*, J. Phys.: Condens. Matter **29**, 254002 (2017).

[21] Y. Wang, J. Lv, L. Zhu, and Y. Ma, Phys. Rev. B **82**, 094116 (2010).

[22] Y. Wang, J. Lv, L. Zhu, and Y. Ma, Comput. Phys. Commun. **183**, 2063 (2012).

[23] J. Lv, Y. Wang, L. Zhu, and Y. Ma, Phys. Rev. Lett. **106**, 015503 (2011).

[24] Y. Wang, H. Liu, J. Lv, L. Zhu, H. Wang, and Y. Ma, Nat. Commun. **2**, 563 (2011).

[25] L. Zhu, H. Liu, C. J. Pickard, G. Zou, and Y. Ma, Nat. Chem. **6**, 644 (2014).

[26] G. Kresse and J. Furthmuller, Phys. Rev. B **54**, 11169 (1996).

[27] G. Kresse and J. Furthmuller, Comput. Mater. Sci. **6**, 15 (1996).

[28] J. P. Perdew, K. Burke, and M. Ernzerhof, Phys. Rev. Lett. **77**, 3865 (1996).

[29] P. E. Blochl, Phys. Rev. B **50**, 17953 (1994).

[30] S. Baroni, P. Giannozzi, and A. Testa, Phys. Rev. Lett. **58**, 1861 (1987).

[31] S. Baroni, S. De Gironcoli, A. Dal Corso, and P. Giannozzi, Rev. Mod. Phys. **73**, 515 (2001).

[32] X. Gonze, Phys. Rev. A **52**, 1096 (1995).

[33] A. Togo, F. Oba, and I. Tanaka, Phys. Rev. B **78**, 134106 (2008).

[34] A. Togo, L. Chaput, I. Tanaka, and G. Hug, Phys. Rev. B **81**, 174301 (2010).

[35] B. Saparov, J. E. Mitchell, and A. S. Sefat, Supercond. Sci. Technol. **25**, 084016 (2012).

[36] Y. Nishihara, Y. Yamaguchi, M. Tokumoto, K. Takeda, and K. Fukamichi, Phys. Rev. B **34**, 3446 (1986).

[37] T. Kikegawa and H. Iwasaki, J. Phys. Soc. Jpn. **56**, 3417 (1987).

[38] See Supplemental Material at http://link.aps.org/supplemental/10.1103/PhysRevB.96.134116 for more detailed computational methods, as well as the formation enthalpies of various CrAs compounds, magnetic and electronic structures of $Pnma$ CrAs, and phonon band structures of $P6_3/mmc$ and $I4_1/md$ phases for CrAs, etc., which includes Ref. [52].

[39] J. Feng, R. G. Hennig, N. W. Ashcroft, and R. Hoffmann, Nature (London) **451**, 445 (2008).

[40] H. Akinaga and M. Mizuguchi, J. Phys.: Condens. Matter **16**, S5549 (2004).

[41] M. Mizuguchi, H. Akinaga, T. Manago, K. Ono, M. Oshima, M. Shirai, M. Yuri, H. J. Lin, H. H. Hsieh, and C. T. Chen, J. Appl. Phys. **91**, 7917 (2002).

[42] M. Mizuguchi, H. Akinaga, T. Manago, K. Ono, M. Oshima, and M. Shirai, J. Magn. Magn. Mater **239**, 269 (2002).

[43] H. Akinaga, T. Manago, and M. Shirai, Jpn. J. Appl. Phys. **39**, L1118 (2000).

[44] R. Podloucky, J. Magn. Magn. Mater. **43**, 291 (1984).

[45] K. Motizuki, K. Katoh, and A. Yanase, J. Phys. C **19**, 495 (1986).

[46] A. D. Becke and K. E. Edgecombe, J. Chem. Phys. **92**, 5397 (1990).

[47] B. Silvi and A. Savin, Nature (London) **371**, 683 (1994).

[48] A. Savin, R. Nesper, S. Wengert, and T. F. Fssler, Angew. Chem., Int. Ed. Engl. **36**, 1808 (1997).

[49] A. Kuc, N. Zibouche, and T. Heine, Phys. Rev. B **83**, 245213 (2011).

[50] S. Lebegue and O. Eriksson, Phys. Rev. B **79**, 115409 (2009).

[51] H. Kotegawa, S. Nakahara, H. Tou, and H. Sugawara, J. Phys.: Condens. Matter **29**, 234002 (2017).

[52] J. Xu, M. Greenblatt, T. Emge, P. Hohn, T. Hughbanks, and Y. Tian, Inorg. Chem. **35**, 845 (1996).